Accepted by ApJ on 8 October 2010

Near-IR H_2 Emission of Protostars: Probing Circumstellar Environments[1]

Thomas P. Greene

NASA Ames Research Center, M.S. 245-6, Moffett Field, CA 94035

tom.greene@nasa.gov

Mary Barsony[2]

Department of Physics and Astronomy, San Francisco State University, 1600 Holloway Drive, San Francisco, CA 94132

mbarsony@SpaceScience.org

and

David A. Weintraub

Department of Physics and Astronomy, Vanderbilt University, Nashville, TN 37235

david.a.weintraub@vanderbilt.edu

ABSTRACT

We present new observations of near-infrared molecular hydrogen (H_2) line emission in a sample of 18 Class I and flat-spectrum low mass protostars, primarily in the Tau-Aur and ρ Oph dark clouds. The line emission is extended by up to several arcseconds (several hundred AU) for most objects, and there is little night-to-night variation in line strength coincident with the continuum point source. Flux ratios of H_2 $v = 2 - 1$ $S(1)$ and $v = 1 - 0$ $S(1)$ lines are consistent with this emission arising in jets or winds in many objects. However, most objects have only small offsets (under 10 km s^{-1}) between their H_2 and photospheric radial velocities. No objects have line ratios which are clearly caused solely by UV excitation, but the H_2 emission of several objects may be caused by UV or X-ray excitation in the presence of circumstellar dust. There are several objects in the sample whose observed velocities *and* line fluxes suggest quiescent, non-mechanical origins for their molecular hydrogen emissions. Overall we find the H_2 emission properties of these protostars to be similar to the T Tauri stars studied in previous surveys.

[2]Space Science Institute, 4750 Walnut Street, Suite 205, Boulder, CO 80301

Subject headings: ISM: jets and outflows — stars: pre-main-sequence, formation — infrared: stars — techniques: spectroscopic

1. Introduction

Embedded low-mass protostars have been identified from their infrared (IR) energy distributions for over two decades, but their high extinctions and relatively small sizes make it very difficult to observe how radiation from the central protostars interacts with their inner, pre-planetary circumstellar disks. Recent high sensitivity, high resolution spectroscopic surveys have revealed the detailed *stellar* properties of significant numbers of these objects (Doppmann et al. 2005; White & Hillenbrand 2004; Greene & Lada 2002), but less is known about the physical conditions in their disks, especially of the gaseous component, or about their inner disks where planets might form and migrate. Here, we explore the gaseous component of the innermost regions of self-embedded (Class I and flat-spectrum; hereafter FS) protostars via high-resolution near-infrared (NIR) spectroscopy of the most abundant molecule in proto-planetary disks, molecular hydrogen (H_2). Near-infrared H_2 transitions are used, since the high extinctions to these sources preclude UV spectroscopy.

The NIR ro-vibrational lines of H_2 are good tracers of physical conditions in inner circumstellar disks and winds close to protostars. There are several different mechanisms that might be responsible for the production of NIR H_2 emission lines in late-stage protostars. These include: *i)* shock heating of the ambient medium by winds or jets, *ii)* X-ray heating, or *iii)* UV-heating, level pumping and fluorescence.

Protostars must accrete mass at mean rates of $\sim 10^{-6} - 10^{-5} M_\odot$ yr^{-1} to assemble themselves on time scales of several 10^5 yr, and these high rates produce significant UV flux when the accreting matter impacts the stellar surface (e.g., Gullbring et al. 2000). Protostars and T Tauri stars are also known to be strong and variable sources of X-ray emission (e.g., Imanishi et al. 2001, 2003; Güdel et al. 2007; Flaccomio et al. 2009). Both UV and X-rays can excite vibrational states of H_2, producing NIR line emission (e.g., Gredel & Dalgarno 1995; Nomura et al. 2007). Many protostars and T Tauri stars also shed mass in jets that drive molecular outflows, and these jets also frequently excite NIR vibrational H_2 line emission (Zinnecker et al. 1998).

The most commonly encountered excitation mechanism for NIR H_2 emission associated with protostars to date has been shock-excitation[2] (e.g., Davis et al. 2010), consistent with many self-

[1]The data presented herein were obtained at the W.M. Keck Observatory from telescope time allocated to the National Aeronautics and Space Administration through the agency's scientific partnership with the California Institute of Technology and the University of California. The Observatory was made possible by the generous financial support of the W.M. Keck Foundation.

[2]See `http://www.jach.hawaii.edu/UKIRT/MHCat/` for an up-to-date listing of "Molecular Hydrogen Emission-Line

embedded protostars being associated with large-scale molecular outflows (e.g., Moriarty-Schieven et al. 1992). These outflows are understood to be driven by powerful stellar winds (Masson & Chernin 1993). Such winds are often detected as blue-shifted absorption components in forbidden emission lines or in the HeI 1.0830 μm line associated with protostars and young T Tauri stars (e.g., Edwards et al. 1993; Kwan et al. 2007). Winds are also believed to cause the shocked IR H_2 emission seen in jets from heavily extinguished young stellar objects. Such stellar winds are inferred to be driven by mass accretion onto young stars. Jets detected in NIR H_2 lines frequently are displaced in space and in radial velocity from photospheric absorption features and usually have relatively large linewidths of a couple dozen km s^{-1} or more. For example, in a recent VLT/ISAAC pilot study of the H_2 1−0 S(1) emission from embedded Class I sources, mean intensity-weighted velocities were blue-shifted by -90 to -10 km s^{-1} and velocity widths of the lines varied from $\sim$ 45 km s^{-1} to $\sim$ 80 km s^{-1} (Chrysostomou et al. 2008).

X-rays and UV may also excite molecular hydrogen emission in the inner circumstellar environments of protostars. Both of these processes offer a radiative alternative to the mechanical excitation excitation of the NIR H_2 emission. If dominant, these excitation mechanisms may produce emission lines with lower velocity widths or offsets than if the H_2 were mechanically excited in shocks or jets. We now consider the mechanisms, observational evidence, and implications for these processes in protostellar environments.

It is now well established that Class I/FS protostars are copious X-ray emitters ($10^{29} \leq L_x \leq 10^{31}$ erg s^{-1}, $\sim$100−1000 times more X-ray luminous than main-sequence stars), and emit higher energy X-rays (4-6 keV vs. 1-2 keV) than their older, T Tauri cousins (e.g., Casanova et al. 1995; Grosso et al. 1997; Imanishi et al. 2001; Feigelson et al. 2007). One would, therefore, expect significant X-ray heating of the disk/inner envelope material surrounding these central objects (e.g., Meijerink et al. 2009, 2007). X-rays from young stellar objects (YSOs) can penetrate disk atmospheres to fairly large surface densities and can ionize circumstellar gas at a level greater than Galactic cosmic rays out to large distances ($\sim 10^4$ AU; Glassgold et al. 2005).

The mechanism of H_2 excitation by X-rays requires impacts from energetic electrons. X-rays impact hydrogen molecules, ejecting electrons. These high energy electrons subsequently collide with and ionize or dissociate ambient gas, losing kinetic energy in the process. Some of electrons will eventually have energies appropriate to excite ambient H_2 molecules into excited states instead of dissociating them completely (e.g., Gredel & Dalgarno 1995; Tine et al. 1997; Maloney et al. 1996). Direct evidence for X-ray heating of gas other than H_2 in disks has been found for several Class I sources in which the 6.4 keV line from neutral iron has been detected (Giardino et al. 2007, and references therein).

Glassgold and co-workers especially have emphasized the importance of X-ray heating of disk atmospheres out to relatively large distances from the central source (Glassgold et al. 2007,

---

Objects (MHOs) in Outflows from Young Stars."

2004). Such heating can extend to large distances because of disk flaring, first proposed to account for the spectral energy distributions (SEDs) produced by dust (Kenyon & Hartmann 1987; Chiang & Goldreich 1997). More recent disk modeling, especially studies involving disk chemistry, routinely use vertically stratified models, with different gas and dust scale heights (d'Alessio et al. 1999; Aikawa et al. 2002; Gorti & Hollenbach 2008; Lacy et al. 2010). In X-ray heated disk models, there is a low column density ($N_H \sim 10^{20}$ cm^{-2}) surface layer of hot (T$\sim$4000 K) gas that extends to $\gtrsim$10 AU radius (Najita et al. 2009).

In the context of disk heating by X-rays, it must be noted that current disk models assume irradiation by a central source with X-ray spectra typical of T Tauri stars: with plasma having kT_X =1 keV and a low-energy cut-off of 100 eV (e.g., Glassgold et al. 2007). However, Class I and FS sources are known to have harder X-ray spectra, with 4 keV $\leq kT_x \leq$6 keV being typical (e.g., Imanishi et al. 2001). Unsurprisingly, the column densities of hydrogen gas inferred towards Class I/FS sources from X-ray observations are $\sim N_H = 1 - 5 \times 10^{22}$ cm^{-2}, 1-2 orders of magnitude greater than inferred for T Tauri stars. Finally, the quantity, L_x/L_{bol}, is systematically smaller for Class I/FS objects relative to T Tauri stars, consistent with the interpretation of higher accretion rates in these systems. The higher accretion rates create higher optical depths in the X-ray absorbing gas, obscuring the lower energy X-rays and producing relatively lower L_x/L_{bol} ratios. Higher accretion rates would also lead to higher heating rates of the disk gas in self-embedded protostars than in classical T Tauri star (CTTS) disks (e.g., d'Alessio et al. 2004).

The possibility of UV excitation of the NIR H_2 lines also exists for Class I/FS protostars, given their consistently higher accretion rates relative to T Tauri stars. The excess UV continuum emission observed in CTTSs has been modeled as being produced by the impact of accretion columns onto the pre-main-sequence stellar surface (e.g., Gullbring et al. 2000). This UV continuum excess could potentially excite molecular hydrogen, producing emission lines in the near-infrared. Strong Lyman-α emission from the central object can irradiate the disk's surface, and, if H_2 is present at $\sim$ 2000K, can excite the H_2 into electronic states which produce a rich UV emission-line spectrum as observed in some T Tauri stars (Herczeg et al. 2006). Finally, if the stellar EUV flux is sufficiently strong, it can ionize hydrogen, which produces high temperatures (T$\approx 10^4$K) and small mean molecular weights at the disk surface. Outside some critical radius, the gas becomes unbound, and a slow, v$\approx$10 km s^{-1}, photoevaporative wind forms (Alexander et al. 2006a,b; Gorti et al. 2009; Woitke et al. 2009).

Like molecular hydrogen, [NeII] emission can also arise from high energy photons in dense circumstellar disks or outflows. [NeII] line emission at 12.81 μm and [NeIII] emission at 15.5 μm was predicted to be detectable in the case of X-ray heated disk gas. The 12.81 μm [NeII] line has subsequently been detected in a number of young stars with the Spitzer Space Telescope (Glassgold et al. 2007; Pascucci et al. 2007; Lahuis et al. 2007; Flaccomio et al. 2009; Najita et al. 2010) and has been studied at high spectral resolution from the ground in three objects (Herczeg et al. 2007; Najita et al. 2009). Although a disk origin has been postulated or confirmed for the [NeII] emission observed in the objects studied at high spectral resolution, there are also sources in which [NeII]

is detected in outflows close to the sources (e.g., Neufeld et al. 2006; van Boekel et al. 2009).

In general, gas motions in the inner circumstellar environments (within ~ 100 AU) of protostars have not been studied well except for a very few cases of velocity resolved NIR CO observations, and this has limited our understanding of how they accrete matter, form winds, shed angular momentum, and disperse their natal circumstellar envelopes. We seek to understand these processes as well as the UV and X-ray radiation environments of their circumstellar disks by embarking on a new study of protostars' NIR H_2 line strengths, morphologies, and velocities.

H_2 NIR ro-vibrational line ratios yield excitation temperatures and also provide clues to excitation mechanisms. The intensity ratio of $S(1)$ lines in the $v = 2 \rightarrow 1$ and $v = 1 \rightarrow 0$ transitions is often used as a diagnostic. This ratio has a value of 0.13 in shocked gas at 2000 K and a value of 0.54 for UV pumping. For X-ray excitation, this ratio is predicted to be 0.06 in gas of low fractional ionization (10^{-4}) and 0.54 in gas of high fractional ionization (10^{-2}) (Gredel & Dalgarno 1995). Any observed variability in these emission lines can also provide clues to the nature of their excitation and the location of the excited and emitting gas.

Several recent studies have made good progress in diagnosing the nature of H_2 excitation in the inner circumstellar disks of CTTSs using observations of their NIR ro-vibrational emission lines. A growing body of work shows that the NIR H_2 line radial velocities and linewidths of many CTTS and Herbig AeBe stars are consistent with UV or X-ray excitation in a circumstellar disk (Weintraub et al. 2000; Bary et al. 2002, 2003; Carmona et al. 2007; Bary et al. 2008). By contrast, in a recently completed NIR adaptive optics (AO) integral field spectroscopic study of several CTTS, the H_2 emissions were most consistent with shocks arising in winds (Beck et al. 2008).

Despite this progress in understanding H_2 emission in CTTSs, little has been done to date in probing the nature of such emission in more embedded Class I and flat–spectrum protostars. Greene & Lada (1996) reported that these protostars were significantly more likely to have NIR H_2 emission than CTTSs, and Doppmann et al. (2005) found that 23 of 52 observed protostars showed NIR H_2 emission. The most embedded protostars also have significant envelopes that may have enough column density to generate observable H_2 emission if the hydrogen molecules there receive sufficient radiative or mechanical energy. If this envelope source existed, it would be a new source of emission not present in CTTSs. Unfortunately, earlier studies did not have adequate spectral resolution or spectral range to observe multiple NIR ro–vibrational lines simultaneously with high spectral resolution and good signal-to-noise: all necessary ingredients for measuring line velocities and line ratios in order to diagnose excitation.

An early motivation for a new observational study was the identification of outflow drivers amongst late-stage protostars via detection of NIR H_2 emission at high spectral resolution observed directly towards the putative powering source (Barsony 2005). However, careful examination of the H_2 $v = 1 - 0$ $S(0)$ line profiles (at 2.2235 μm) observed at R$\sim$17,000 in the work of Doppmann et al. (2005), showed that a substantial number of sources exhibited relatively narrow linewidths

($\Delta v \leq 15$ km s^{-1}). Furthermore, in many cases, the H_2 emission line centers were not significantly displaced from the central object's radial velocity. Taken together, these two observations call into question an outflow origin for the observed NIR H_2 emission in some sources.

We have conducted a new study of Class I and flat-spectrum protostars with data sufficient for diagnosing the natures of their H_2 emission in their inner circumstellar disks and envelopes. We report on the sample and observations in §2 and present our analysis of these data in §3. We discuss our results in §4 and summarize our work in §5.

2. Observations and Data Reduction

High resolution NIR spectra of 18 Class I and flat-spectrum protostars previously searched for H_2 $v = 1 - 0$ $S(0)$ emission by Doppmann et al. (2005) were re-observed with the Keck II telescope on Mauna Kea, Hawaii using its NIRSPEC multi-order cryogenic echelle facility spectrograph (McLean et al. 1998). This included 17 objects found to exhibit H_2 $v = 1 - 0$ $S(0)$ emission in this previous study, and one (03260+311A) without. All new spectra were acquired on 2007 June 24 and 25 UT (ρ Oph and Ser objects) and 2008 January 24 and 25 (Tau-Aur and Per objects). The late type (K1 – M2.5) dwarfs HD 20165, HD 28343, and HD 285968 with precision velocities measured by Nidever et al. (2002) were observed on 2008 January 24 UT to serve as radial velocity references.

Spectra were acquired with a 0.″58 (4-pixel) wide slit, providing spectroscopic resolution $R \equiv \lambda/\delta\lambda = 18{,}000$ (16.7 km s^{-1}). The plate scale was 0.″20 pixel^{-1} along the 12″ slit length, and the seeing was typically 0.″5–0.″6. The NIRSPEC gratings were oriented to observe the 2.1218 μm H_2 $v = 1 - 0$ $S(1)$, 2.2477 μm H_2 $v = 2 - 1$ $S(1)$, and 2.386 μm H_2 $v = 3 - 2$ $S(1)$ lines on the instrument's 1024 × 1024 pixel InSb detector array in a single exposure. The 2.2233 μm H_2 $v = 1-0$ $S(0)$ line previously observed by Doppmann et al. (2005) was also captured in this grating setting. The NIRSPEC-7 blocking filter was used to image these orders on the detector. NIRSPEC was configured to acquire simultaneously multiple cross-dispersed echelle orders 32–37 (2.05–2.40 μm, non-continuous) for all objects. Each order had an observed spectral range $\Delta\lambda \simeq \lambda/67$ ($\Delta v \simeq 4450$ km s^{-1}).

The slit was held physically stationary during the exposures and thus rotated on the sky as the non-equatorially-mounted telescope tracked when observing. Data were acquired in pairs of exposures of durations from 180–600 s each, with the telescope nodded 3″ or 6″ along the slit between frames so that object spectra were acquired in all exposures. Most of the targets were observed twice on consecutive nights. The observation dates, total integration times, slit angles and coordinates of all Class I and flat-spectrum objects are given in Table 1. The early-type (B9–A0) dwarfs HD 28354, HR 6070, HR 5993, and HD 168966 were observed for telluric correction of the target spectra. The telescope was automatically guided with frequent images from the NIRSPEC internal "SCAM" IR camera during all exposures of more than several seconds duration. Spectra

of the internal NIRSPEC continuum lamp were taken for flat fields, and exposures of the Ar, Ne, Kr, and Xe lamps were used for wavelength calibrations.

All data were reduced with IRAF. First, object and sky frames were differenced and then divided by normalized flat fields. Next, bad pixels were fixed via interpolation, and spectra were extracted with the APALL task. Spectra were wavelength calibrated using low-order fits to lines in the arc lamp exposures, and spectra at each slit position of each object were co-added. Instrumental and atmospheric features were removed by dividing wavelength-calibrated object spectra by spectra of early-type stars observed at similar airmass at each slit position. Final spectra were produced for each night by combining the spectra of both slit positions for each object and then multiplying them by spectra of 10,000 K blackbodies to rectify the spectral shapes induced when dividing by the telluric stars with that effective temperature. Spectra acquired on different nights were not combined in any way.

3. Analysis and Results

The spectra of all objects in Table 1 were analyzed by measuring their H_2 $v = 1 - 0$ $S(1)$, $v = 2 - 1$ $S(1)$, and $v = 1 - 0$ $S(0)$ line fluxes, H_2 line radial velocities, and the radial velocities of photospheric absorption lines. The 2.386 μm H_2 $v = 3 - 2$ $S(1)$ line is in a region of poor atmospheric transmission and was not significantly detected in any object. The values of the H_2 line properties and their night-to-night variations were analyzed for physical insights into their excitation as described in this section.

Spectra of the H_2 $v = 1 - 0$ $S(1)$ region are shown for all objects in Figure 1; the first epoch (2007 Jun 24 and 2008 Jan 24) is shown in the left panel and the second (2007 Jun 25 and 2008 Jan 25) in the right. Of the 18 objects, 14 were observed in both epochs. When present, the $v = 1 - 0$ $S(1)$ line was the strongest H_2 feature observed in all objects. All emission spectra shown in the figures and all derived strength and velocity values presented in Table 2 are for the H_2 emission that was spatially coincident with each object's continuum source, typically limited by the $0\farcs6$ seeing, corresponding to a spatial extent of ~ 100 AU for most sources.

3.1. H_2 Emission Morphologies

The spatial extent of the H_2 emission along the spectrograph slit was measured for each object by examining the differenced and flat-fielded spectral images that were created prior to spectral extraction. The non-rotating spectrograph slit was projected onto the sky at different position angles each night, so the two observational epochs sample the spatial extent of any extended emission differently (see position angles in Table 1).

The angular extent of the H_2 emission along the length of the slit is reported in Table 2) for

each observation. Ten of the 18 protostars showed H_2 emission that was over $1''$ in spatial extent in at least one observation (at least one position angle). Of the 14 objects observed in two epochs, 6 had H_2 $v = 1-0$ $S(1)$ emission extended by $\sim 1''$ or less on both nights. Therefore the molecular hydrogen emission of these 6 objects is contained within about 70 AU ($\sim 0\farcs5$) of their central stars. The highest H_2 surface brightness was generally found to be coincident with each object's unresolved point source, but in some cases the extended emission may have more integrated flux and luminosity than the point source component. Beck et al. (2008) found this to be true in their AO integral field study of several CTTSs that sampled their immediate circumstellar environments completely instead of evaluating just two slit position angles as done in this study.

Objects with significantly different spatial extents between epochs (position angles) may have their H_2 emission confined to asymmetrical structures like jets. 03260+3111B, 04158+2805, and 04264+2433 are examples of objects with these potentially jet-like morphologies. 03260+3111A shows significantly extended emission, but this is spatially displaced from the stellar continuum which has no coincident H_2 emission.

3.2. Variability

We found H_2 emission in all of the 17 objects also found to have H_2 emission at earlier epochs by Doppmann et al. (2005). The one source without emission (03260+3111A) in that earlier study also did not show H_2 emission in our new observations. This indicates that these these protostars do not terminate or initiate their H_2 emissions on time scales as short as 5 – 10 years, suggesting that their H_2 lines are emitted over physically large regions or else are excited by processes with relatively stable fluxes.

Fourteen of the 18 objects were observed twice, with the two observations spaced approximately 24 hr apart. The position angles of both observations were sometimes similar (within ~ 10 deg), but often they varied by 60 deg or more (Table 1). Therefore the different slit position angles must be considered when comparing H_2 line fluxes measured on the different dates to determine whether any differences are due to true temporal variation or the rotation of different spatial features (i.e., jets) onto or off of the slit. However, the measured equivalent H_2 emission widths and line velocities were similar for both observations of each object (see Table 2), so there appears to be little temporal variation on ~ 1 day time scales for the emission that is spatially confined to be coincident with the protostar continuum source confined within the slit width.

3.3. Radial Velocities and Line Widths

Stellar photospheric radial velocities were computed from the continuum absorption lines of all observed objects. First, the object spectra were cross-correlated (using fxcor in IRAF) with spectra of the radial velocity standards, always HD 28343 (K7 V) and sometimes HD 20165 (K1

V) or HD 285968 (M2.5 V), using up to 4 spectral orders that contained photospheric lines but no emission lines. Heliocentric V_{LSR} radial velocities were computed for each object by summing the radial velocity shift measured with the cross-correlations, the mean measured radial velocities of the 3 standards (Nidever et al. 2002), and the V_{LSR} corrections for the objects and standards at their time of observation (from the IRAF rvcorrect task). The V_{LSR} radial velocities computed in this way generally agreed well with those of the 10 objects also reported by Covey et al. (2006). We observed these 10 objects a total of 18 times, and we measured the offset from the Covey et al. (2006) velocities to be 2.2 ± 3.5 km s^{-1}. This offset is consistent with zero, and the standard deviation is not surprising given the 17 km s^{-1} spectral resolution and the generally heavily veiled spectra.

Radial velocities of H_2 lines were computed by measuring the central wavelengths of Gaussian profiles fit to the lines using the IRAF splot task and then converting these values to velocities. These observed radial velocities were converted to V_{LSR} values by adding the V_{LSR} correction offset computed for each object as described above. The velocities of the H_2 lines relative to photospheric lines of each object were computed by differencing these two V_{LSR} radial velocities, and the results are shown in Table 2 and Figure 2. FWHM velocity widths of the $v = 1 - 0$ $S(1)$ lines were computed by subtracting the instrumental line width of 17 km s^{-1} in quadrature from the FWHM values of the Gaussian fits. These resultant line widths are also reported in Table 2, and their histogram is shown in Figure 3. Objects observed twice on successive nights had similar radial and FWHM velocities (Table 2), so these values were averaged to reduce noise in Figures 2 and 3. The other H_2 lines generally had similar FWHM values, but the $v = 1 - 0$ $S(1)$ lines had the highest signal-to-noise, so only those values are presented. We estimate that all reported velocities have uncertainties of a few km s^{-1}.

3.4. H_2 Line Fluxes and Ratios

Line luminosities were estimated by scaling the relative fluxes measured in each H_2 line to the spatially coincident 2.2 μm continuum and multiplying this by the absolute 2.2 μm continuum flux estimated from each object's 2MASS K-band magnitude after correcting for extinction. Extinctions were calculated by de-reddening each object's JHK 2MASS magnitudes to the CTTS locus (Meyer et al. 1997). Extinctions were estimated at each H_2 line wavelength using $A_v = 9.09[(J-H)-(J-H)_0]$, $A_k = 0.09A_v$, and $A_\lambda \propto \lambda^{-1.9}$. These values were computed by and derived from Cohen et al. (1981) for the CIT photometric system, which is essentially identical to that of 2MASS (Carpenter 2001).

Distances were assumed to be 140 pc for Tau-Aur (Kenyon et al. 1994), 140 pc for ρ Oph (Mamajek 2008), 260 pc for SVS 2 in Serpens (Straižys et al. 1996), and 320 pc for the 03260+3111 objects in Perseus (Herbig 1998). H_2 line equivalent widths and luminosities are presented in Table 2, and a histogram of luminosities of the H_2 $v = 1 - 0$ $S(1)$ line is shown in Figure 4. A histogram of H_2 $1 - 0/2 - 1$ $S(1)$ line ratios is presented in Figure 5. As done in previous figures,

values derived from observations of objects acquired on successive nights are averaged in these figures as well. Note that the H_2 line ratio value plotted in Figure 5 is the inverse of the values presented in Table 2 (column 8).

3.5. Correlations

We examined whether correlations exist between measured H_2 line properties and other protostellar activity indicators in an attempt to isolate the origins of the H_2 line emissions.

First we computed the correlations between the H_2 line properties measured in this new survey. The FWHM velocity widths and the $1-0/2-1$ $S(1)$ line ratios in Table 2 have a correlation coefficient of 0.61, which improves to 0.71 when both observations of a single object are averaged into single points. This value drops to only 0.17 (individual or mean values) if the observations of 03260+3111B are excluded; its high FWHM velocity and relatively high $1-0/2-1$ $S(1)$ line ratio drives this correlation. Thus the object sample as a whole does not show a good correlation between its H_2 FWHM velocities and $1-0/2-1$ $S(1)$ line ratios. We then examined correlations between H_2 FWHM velocities and velocity offsets between H_2 and photospheric lines. These values had correlation coefficients of -0.43 and -0.47 for individual and averaged values, respectively. The square of the correlation coefficient is below 0.25 in both cases, indicating that less than 25% of the variance of the two quantities are in common for this sample of protostars, a poor correlation.

Next we correlated the protostars' H_2 line properties with other physical characteristics measured in other studies. Twelve of the 18 objects have measured X-ray luminosities or upper limits (Güdel et al. 2007; Flaccomio et al. 2009), and the correlation coefficient between the logarithms of their H_2 $1-0$ $S(1)$ line luminosities and the logarithms of their X-ray luminosities is -0.20, suggesting a very weak or nonexistent inverse correlation between these properties. Finally, we re-analyzed the spectra of Doppmann et al. (2005) and used their equivalent width measurements of H_2 $1-0$ $S(0)$ and HI Br γ emission lines to evaluate the correlation of these properties in that somewhat earlier epoch. We found that these values had a correlation coefficient of 0.20, indicating another poor correlation. In summary, we find little correlation among the NIR H_2 line emission properties or between these properties and other young stellar activity indicators.

4. Discussion

The different radiative and collisional excitation mechanisms of H_2 are well matched to the radiative and mass flux processes in the environments of protostars and T Tauri stars. We now interpret the results of the preceding analysis in terms of several of these possible processes in order to constrain the H_2 excitation mechanisms of the sample and to understand better the circumstellar environments of these protostars.

4.1. Emission Morphologies, Variability, and Velocities

In addition to their compact H_2 line emissions, all but 4 of the 18 objects also showed $v = 1 - 0$ $S(1)$ molecular hydrogen emission extended by $\sim 1''$ or more along the slit (see Table 2), corresponding to 70 AU ($\sim 0\farcs5$) or more projected radial distance. It is unlikely that UV radiation could travel that far from the central protostars without significant attenuation by gaseous and dusty envelopes, so it is likely that this extended emission is excited by either stellar winds or high energy X-rays. The expected small size of the UV emission region on the protostellar photosphere also suggests that UV may not be a good candidate for exciting the observed steady and long-lived H_2 line emissions. Two objects, GY 21 and IRS 43, have extended $1 - 0$ $S(1)$ emission with broad line widths, FWHM $\gtrsim$ 40 km s^{-1}, about twice that of the compact emission spatially coincident with their stellar continua. The extended emissions of these 2 objects are good candidates for excitation in shocks caused by stellar winds.

The relatively stable values of the point source H_2 emission over 1 day and several-year time scales (see §3.2 and Table 1) also provide clues to the nature of these emissions. Numerous Class I and FS protostars have been observed to undergo rapid (several hr), large amplitude X-ray emission variations (e.g., Imanishi et al. 2001, 2003; Güdel et al. 2007; Flaccomio et al. 2009). This X-ray flaring of several protostars (e.g., IRS 43) has also been observed to appear or disappear in data taken $\sim$ 5 – 10 years apart. If these X-ray flares were exciting H_2 close to the stars, then it is likely that we would see significant night-to-night or year-to year variations in their point-source near-IR line fluxes, but this is not seen in our data. The very stable observed molecular hydrogen emission is more consistent with mechanical (wind or jet) excitation as well as excitation by steady, non-flaring X-ray emission from the protostars.

The preceding analysis of the velocity widths and velocity shifts of the H_2 line emission in §3.3 also provides clues to the nature of its excitation. Collisional excitations in jets or winds are likely to result in H_2 emission line radial velocities displaced from photospheric absorption lines by over 10 km s^{-1}, exhibition of broad line wings, or large full-width half maximum velocities of several 10 km s^{-1} or more (Maloney et al. 1996; Montmerle et al. 2000; Nomura et al. 2007; Beck et al. 2008). Jets are also often significantly collimated and spatially extended, making them easy to identify in one or two dimensional spectral images (e.g., Schwartz & Greene 2003).

The significant spatial extension of the H_2 line emission of many objects is consistent with collisional excitation in winds or by jets. However, only 5 of 13 protostars show radial velocity offsets between their H_2 lines and photospheric absorption lines with absolute value of greater than 4 km s^{-1} (see Fig. 2). This value is similar to the 3.5 km s^{-1} uncertainty we measured for radial velocity standards (see §3.3), so we do not consider velocity offsets less than 4 km s^{-1} to be significant. Only 3 protostars have velocity offsets of at least 10 km s^{-1}, significant at about the 3-σ confidence level or greater. This evidence suggests that collisional excitation in jets is unlikely to be the molecular hydrogen excitation mechanism in most objects (except the 3 with significant velocity differences).

However, the on-source H_2 $v = 1 - 0$ $S(1)$ line FWHM line widths of all 17 protostars with this on-source feature are broader than 10 km s^{-1} (see Fig. 3). Six of the emitting objects (35%) exhibit FWHM greater that 20 km s^{-1}. All 6 of these objects also show spatially extended H_2 emission many tens of AU from their central stars; this combination of factors makes them good candidates for collisional excitation in jets or winds. Seven of the emitting objects (41%) have FWHM line widths below 16 km s^{-1}. This is similar to the 9 to 14 km s^{-1} line widths found by Bary et al. (2003) and Bary et al. (2008) for 8 of 10 T Tauri stars found to have H_2 emission, which they interpreted as evidence for quiescent emission in circumstellar disks. We conclude that the molecular hydrogen emission line velocities and FWHM values of at least 3 to 6 of the 17 emitting objects are consistent with collisional excitation in jets, and at least 7 or 8 objects have H_2 velocity parameters consistent with quiescent (non-collisional) excitation.

4.2. Emission Line Strengths and Ratios

NIR vibrational H_2 line ratios are also sensitive to the gas excitation levels and excitation mechanisms. Gredel & Dalgarno (1995) show that the ratios of the H_2 $v = 1 - 0$ $S(1)$ to $v = 2 - 1$ $S(1)$ lines are relatively sensitive to excitation mechanisms. They compute the ratios of these 2 lines to be 1.9 for UV excitation, 7.7 for shocked gas at $T = 2000$ K, and 16.7 for X-ray excitation of low ionization H_2. Black & van Dishoeck (1987) also found similar differences between UV and shock excitation of H_2. However, there are limits to the usefulness of these ratios as diagnostics of excitation in circumstellar disks. In practice it is difficult to distinguish between shocked and X-ray excited H_2 emission from examining only a few NIR lines. Collisions will thermalize the excitation levels of H_2 in a sufficiently dense gas, so $v = 1-0$ $S(1)$ to $v = 2-1S(1)$ line ratios indicative of cold-to-warm gas in equilibrium are not always useful for distinguishing between excitation mechanisms (Gredel & Dalgarno 1995; Maloney et al. 1996; Tine et al. 1997; Nomura et al. 2007; Beck et al. 2008).

However, these line ratios may be useful for diagnosing excitation processes in extreme cases. Black & van Dishoeck (1987) note that fluorescent UV excitation of H_2 produces significant population of vibrational levels $v \geq 2$ and therefore strong emission in the $v = 2 - 1$ $S(1)$ line when not thermalized in a high density environment. This level population can be characterized by a temperature of $T_{\rm vib} \approx 6000 - 9000$ K, much larger than the $T_{\rm vib} = T \simeq 2000$ K characteristic of shock excitation. Therefore any objects with observed ratios of H_2 $v = 1 - 0$ $S(1)$ to $v = 2 - 1$ $S(1) \simeq 2$ $(2 - 1/1 - 0 \simeq 0.5)$ may be exhibiting UV-excited H_2 emission. However, there are no objects in our sample with H_2 $v = 2 - 1/1 - 0$ $S(1) > 0.25$, so we do not have any good candidates for purely UV excitation in a dust-free environment as modeled by Black & van Dishoeck (1987).

The presence of dust grains can significantly alter these ratios and complicate their interpretation. Nomura et al. (2007) have computed the expected NIR H_2 line fluxes for conditions in circumstellar disks around young stars, modeling X-ray and UV heating in the presence of both gas and dust and accounting for thermalization at high gas densities. They find that the H_2 $v = 2 - 1$

$S(1)$ to $v = 1 - 0$ $S(1)$ line ratio is greatly impacted by the presence of dust grains of different sizes (see their Figure 17). For UV excited emission, Nomura et al. (2007) find that this line ratio is $\simeq 0.025$ for a power law dust grain distribution with a maximum size of 10 μm - 1 mm, roughly consistent with that expected for a protostar's circumstellar disk. They find that the grains must be much larger ($\sim$ 10 cm or more) for this ratio to approach the dust-free value of 0.5 computed by Gredel & Dalgarno (1995). This line ratio is much less sensitive to grain size in the case of X-ray excitation; Nomura et al. (2007) find that this value is close to the Gredel & Dalgarno (1995) value of 0.06 for a maximum grain size of 10 μm - 10 cm. Thus they find that the H_2 $v = 2 - 1$ $S(1)$ to $v = 1 - 0$ $S(1)$ line ratio differs by only about a factor of 2 for a circumstellar disk with a power law grain size distribution with a maximum size 10 μm - 1 mm. Nomura et al. (2007) do not consider collisional excitation by winds or jets, but collisional excitation may produce a fairly wide range of gas temperatures and H_2 line ratios as discussed previously.

If excited by collisions in shocks, ratios of the $v = 1 - 0$ $S(1)$ to $v = 1 - 0$ $S(0)$ emission lines can be used to estimate ortho:para ratios of molecular hydrogen and to assess the thermal history of the emitting gas. The values of ortho:para ratios were modeled for C- and J-type shocks by Wilgenbus et al. (2000); see also their summary of previous work. Kristensen et al. (2007) and Harrison et al. (1998) showed that the $v = 1 - 0$ $S(1)$ to $v = 1 - 0$ $S(0)$ emission line ratio directly yields the molecular hydrogen ortho:para ratio with little sensitivity to H_2 rotation temperature. Using Eq. 5 of Kristensen et al. (2007) and assuming an H_2 rotation temperature of 3500 K, we find that the mean ortho:para ratio for our object sample is $< o/p >= 3.2 \pm 0.8$. Hydrogen atom exchanges in shocks set the high temperature limit to o/p ≤ 3 (e.g., see Wilgenbus et al. 2000). Thus it appears that not all objects in our sample have molecular hydrogen emission consistent with production in shocks since a number of objects have o/p > 3. Unfortunately we were unable to use line ratios to diagnose the nature of the spatially extended H_2 emissions seen in many objects (see Table 2 and §4.1). This emission was generally much weaker than the point source emission, and it was not detected significantly in any NIR H_2 line except $v = 1 - 0$ $S(1)$ for any object.

4.3. Molecular Hydrogen Excitation Mechanisms in Observed Protostars

Our sample has 5 objects with H_2 $v = 2 - 0$ $S(1)$ to $v = 1 - 0$ $S(1)$ line ratios in the 0.025 - 0.06 range, consistent with UV or X-ray excitation in the presence of dust. Of these, 04264+2433, 04295+2251, 04365+2535, and IRS 43 have relatively low mean H_2 $v = 1 - 0$ $S(1)$ line widths, FWHM $\lesssim 15$ km s^{-1}. All but 04264+2433 have been detected in X-rays, so X-ray or UV excitation may be possible for these protostars. WL 12 is the other protostar with a line ratio in this range, and it has a broad FWHM $\simeq 30$ km s^{-1} and is associated with a molecular outflow (Bontemps et al. 1996). Therefore its H_2 may be collisionally excited. However, WL 12 has ortho:para ratios of about 4.5, larger than the o/p ≤ 3 limit that can be produced in C-shocks or J-shocks. The objects 04158+2805, 04181+2654, and WL 6 also have estimated o/p ≥ 3.5, indicating non-shock excitation even if their H_2 rotation temperature is somewhat higher than the assumed 3500 K. Therefore the

NIR H_2 emission of these objects may not be excited in jets. The latter 3 objects also have H_2 radial velocity offset by less than 5 km s^{-1} from their photospheric velocities. However, 04158+2805 and 04181+2654 have H_2 FWHM line widths $\geq$ 20 km s^{-1}, clouding a non-mechanical interpretation of their molecular hydrogen excitation.

Interestingly, there are several objects in the sample whose observed velocities *and* line fluxes suggest quiescent, non-mechanical origins for their molecular hydrogen emissions. 04361+2547, WL 6, and IRS 67 all have small H_2 FWHM line widths, small H_2 velocity offsets from photospheric velocities, and small H_2 emission spatial extents (See Table 2). Interestingly, at least one measurement of the $v = 1-0$ $S(1)$ to $v = 2-1$ $S(1)$ line ratios is $\sim$0.07 for each object, similar to the value of 0.06 computed by Gredel & Dalgarno (1995) and Nomura et al. (2007) for X-ray excitation of H_2. Thus these objects appear to be the best candidates for non-mechanical excitation of their molecular hydrogen emissions.

We conclude this discussion by noting that several of the protostars have NIR ro-vibrational emission properties consistent with collisional excitation, and some others appear to be good candidates for X-ray and / or UV excitation. This is similar to the results found by Beck et al. (2008) and Bary et al. (2008) in their surveys of T Tauri stars. We also find no individual or set of spectral features that are inconsistent with previous observations of NIR H_2 emission in CTTSs. It appears that there is no single NIR line diagnostic that can clearly identify the excitation mechanisms of H_2 in the circumstellar disks and environments of protostars, and correlations between diagnostics are not strong (§3.5). However, the measures of emission line morphologies, velocity widths, velocity shifts, and line ratios can constrain the various emission mechanisms when interpreted within an appropriate theoretical model.

5. Summary

We present new observations of near-infrared H_2 line emission in a sample of 18 Class I and flat-spectrum low mass protostars, primarily in the Tau-Aur and ρ Oph dark clouds. We reach the following conclusions from analyzing these data:

1. All 17 objects found to have NIR H_2 ro-vibrational line emission spatially conincident with their continuum sources in an earlier epoch were also found to have this emission in this new study, 5 – 10 years later. There appears to be little temporal variation of this emission on $\sim$ 1 day time scales. Ten of the 18 protostars showed H_2 $v = 1-0$ $S(1)$ line emission that was over $1''$ in spatial extent in at least one observation (at least one position angle).

2. Nearly all of the protostars have H_2 $v = 1-0$ $S(1)$ line emission radial velocities within 10 km s^{-1} of their stellar photospheric line velocities; only 3 objects have H_2 velocity offsets greater than or equal to 10 km s^{-1}. This evidence suggests that collisional excitation in jets is unlikely to be the molecular hydrogen excitation mechanism in many objects.

3. The H_2 $v = 1-0$ $S(1)$ line FWHM line widths of all 17 protostars with this feature on-source are broader than 10 km s^{-1} (Fig. 3). Six of the emitting objects (35%) exhibit FWHM greater that 20 km s^{-1}, and these are good candidates for collisional excitation in jets or winds. Seven of the emitting objects (41%) have point source FWHM line widths below 16 km s^{-1}. The spatially extended H_2 $v = 1 - 0$ $S(1)$ line emission of two objects had line widths FWHM $\gtrsim$ 40 km s^{-1}, about twice that of their central point source emission. This is consistent with collisional excitation by jets or winds.

4. The molecular hydrogen emission line velocities and FWHM values of at least 3 to 6 of the 17 objects with on-source emission are consistent with collisional excitation in jets. At least 7 or 8 objects have H_2 velocity parameters consistent with quiescent (non-collisional) excitation. There are several objects whose small emission line widths, small H_2 – photospheric radial velocity differences, and small spatial extents are more consistent with quiescent molecular hydrogen emission and not collisional excitation.

5. Several of the protostars have H_2 $v = 2 - 0$ $S(1)$ to $v = 1 - 0$ $S(1)$ line ratios indicative of X-ray or UV excitation (in the presence of dust) and are known X-ray emitters. 04361+2547, WL 6, and IRS 67 are the best examples of such protostars. However, we see no rapid variation in the H_2 $\Delta v = 1$ $S(1)$ line fluxes on $\sim$24 hr time scales as might be expected from excitation by X-ray flaring events.

6. We find that the mean ortho:para ratio for our object sample is $< o/p >= 3.2 \pm 0.8$. Hydrogen atom exchanges in shocks set the high temperature limit to o/p ≤ 3 (e.g., see Wilgenbus et al. 2000). Thus it appears that not all objects in our sample have molecular hydrogen emission consistent with production in shocks since a number of objects have o/p > 3. 04158+2805, 04181+2654, WL 6, and WL 12 are all estimated to have ortho:para ratios significantly higher than this value. However, WL 6 is the only protostar with H_2 line ratios and velocities also indicative of non-mechanical excitation.

We thank D. Hollenbach and U. Gorti for helpful discussions of our data and its interpretation via theoretical models. We also thank G. Herczeg for discussing pre-publication data and thank the anonymous referee for thoughtful suggestions that improved this paper. The Keck Observatory Observing Assistants H. Hershley and C. Parker are thankfully acknowledged for assistance with the observations. The authors wish to recognize and acknowledge the very significant cultural role and reverence that the summit of Mauna Kea has always had within the indigenous Hawaiian community. We are most fortunate to have the opportunity to conduct observations from this mountain. TPG acknowledges support from NASA's Origins of Solar Systems program via WBS 811073.02.07.01.89. MB and TPG would like to acknowledge NASA support via NExScI for travel expenses to the W.M. Keck Observatory for acquiring the observations for this project.

Facilities: Keck (NIRSpec), IRAF, 2MASS

REFERENCES

Aikawa, Y., van Zadelhoff, G.J., van Dishoeck, E.F., & Herbst, E. 2002, A&A, 386, 622

Alexander, R.D., Clarke, C.J., & Pringle, J.E. 2006a, MNRAS, 369, 216

Alexander, R.D., Clarke, C.J., & Pringle, J.E. 2006b, MNRAS, 369, 229

Bary, J. S., Weintraub, D. A., & Kastner, J. H. 2002, ApJ, 576, L73

Bary, J. S., Weintraub, D. A., & Kastner, J. H. 2003, ApJ, 586, 1136

Bary, J. S., Weintraub, D. A., Shukla, S., Leisenring, J.M., & Kastner, J. H. 2008, ApJ, 678, 1088

Barsony, M. 2005, in "High-Resolution Infrared Spectroscopy in Astronomy," Proc. of an ESO Workshop held at Garching, Germany, 18-21 November 2003, eds. Käufl, H.U., Siebenmorgen, R., & A. Moorwood, pp.125-130

Beck, T. L., McGregor, P. J., Takami, M., & a, T.-S. 2008, ApJ, 676, 472

Black, J. H., & van Dishoeck, E. F. 1987, ApJ, 322, 412

Bontemps, S., Andre, P., Terebey, S., & Cabrit, S. 1996, A&A, 311, 858

Burton, M. G., Brand, P. W. J. L., a, T. R., & Webster, A. S. 1989, MNRAS, 236, 409

Carmona, A., van den Ancker, M.E., Henning, Th., Goto, M., Fedele, D., & Stecklum, B. 2007, A&A, 476, 853

Carpenter, J. M. 2001, AJ, 121, 2851

Casanova, S., Montmerle, T., a, E. D., & Andre, P. 1995, ApJ, 439, 752

Chiang, E.I. & Goldreich, P. 1997, ApJ, 490, 368

Chrysostomou, A., Bacciotti, F., Nisini, B., Ray, T.P., Eislöffel, J., Davis, C.J., & Takami, M. 2008, A&A, 482, 575

Cohen, J. G., a, S. E., Elias, J. H., & aa, J. A. 1981, ApJ, 249, 481

Covey, K. R., Greene, T. P., Doppmann, G. W., & a, C. J. 2006, AJ, 131, 512

d'Alessio, P., Calvet, N., Hartmann, L., Lizano, S., & Cantó, J. 1999, ApJ, 527, 893

d'Alessio, P., Calvet, N., Hartmann, L., Muzerolle, J., & Sitko, M. 2004, in *Star Formation at High Angular Resolution*, IAU Symp. 221, 403, eds. M.G. Burton, R. Jayawardhana, & T.L. Bourke

Davis, C.J., Gell, R., Khanzadyan, T., Smith, M.D., & Jenness, T. 2010, A&A, 511, 24

Doppmann, G. W., Greene, T. P., Covey, K. R., & Lada, C. J. 2005, AJ, 130, 1145

Edwards, S., Ray, T., & Mundt, R. 1993, Protostars and Planets III, 567

Feigelson, E., Townsley, L., Güdel, M., & Stassun, K. 2007, Protostars and Planets V, 313

Flaccomio, E., Stelzer, B., Sciortino, S., Micela, G., Pillitteri, I., & Testi, L. 2009, A&A, 505, 695

Giardino, G., Favata, F., Pillitteri, I., Flaccomio, F., Micela, G., & Sciortino, S. 2007, A&A, 475, 891

Glassgold, A.E., Feigelson, E.D., Montmerle, T., & Wolk, S. 2005, ASP Conf. Ser. 341, p.165

Glassgold, A.E., Najita, J.R., Igea, J. 2007, ApJ, 656, 515

Glassgold, A.E., Najita, J.R., Igea, J. 2004, ApJ, 615, 972

Gorti, U. & Hollenbach, D. 2008, ApJ, 683, 287

Gorti, U., Dullemond, C.P., & Hollenbach, D. 2009, ApJ, 705, 1237

Gredel, R., & a, A. 1995, ApJ, 446, 852

Greene, T. P., & Lada, C. J. 1996, AJ, 112, 2184

Greene, T. P., & Lada, C. J. 2002, AJ, 124, 2185

Grosso, N., Montmerle, T., Feigelson, E. D., André, P., Casanova, S., & Gregorio-Hetem, J. 1997, Nature, 387, 56

Güdel, M., et al. 2007, A&A, 468, 353

Gullbring, E., Calvet, N., Muzerolle, J., & Hartmann, L. 2000, ApJ, 544, 927

Harrison, A., Puxley, P., Russell, A., & Brand, P. 1998, MNRAS, 297, 624

Herbig, G. H. 1998, ApJ, 497, 736

Herczeg, G. J., Najita, J. R., Hillenbrand, L. A., & Pascucci, I. 2007, ApJ, 670, 509

Herczeg, G. J., Linsky, J. L., Walter, F. M., Gahm, G. F., & Johns-Krull, C. M. 2006, ApJS, 165, 256

Imanishi, K., Koyama, K., & Tsuboi, Y. 2001, ApJ, 557, 747

Imanishi, K., Nakajima, H., Tsujimoto, M., Koyama, K., & Tsuboi, Y. 2003, PASJ, 55, 653

Kenyon, S. J., Dobrzycka, D., & Hartmann, L. 1994, AJ, 108, 1872

Kenyon, S. J., & Hartmann, L. 1987, ApJ, 323 714

Kristensen, L. E., Ravkilde, T. L., Field, D., Lemaire, J. L., & Pineau Des Forêts, G. 2007, A&A, 469, 561

Kwan, J., Edwards, S., & Fischer, W. 2007, ApJ, 657, 897

Lacy, J.H., Harrold, S.T., Watson, D.M. 2010, BAAS, 41, 346

Lahuis, F., van Dishoeck, E.F., Blake, G.A., Evans, N.J. II, Kessler-Silacci, J.E., & Pontopiddan, K.M. 2007, ApJ, 665, 492L

Maloney, P. R., Hollenbach, D. J., & Tielens, A. G. G. M. 1996, ApJ, 466, 561

Mamajek, E. E. 2008, Astronomische Nachrichten, 329, 10

Masson, C. R., & Chernin, L. M. 1993, ApJ, 414, 230

McLean, I. S. et al. 1998, Proc. SPIE, 3354, 566

Meyer, M. R., Calvet, N., & Hillenbrand, L. A. 1997, AJ, 114, 288

Montmerle, T., Grosso, N., Tsuboi, Y., & Koyama, K. 2000, ApJ, 532, 261

Moriarty-Schieven, G. H., Wannier, P. G., Tamura, M., & Keene, J. 1992, ApJ, 400, 260

Meijerink, R., Poelman, D.R., Glassgold, A.E., Najita, J.R., Tielens, A.G.G.M., & Spaans, M. 2009, "The Evolving ISM in the Milky Way and Nearby Galaxies," Proc. of the 4th Spitzer Science Center Conference, eds. K. Sheth, A. Noriega-Crespo, J. Ingalls, & R. Palladini, on-line at http://ssc.spitzer.caltech.edu/mtgs/ismevol/

Meijerink, R., Glassgold, A., & Najita, J. 2007, in "The Spirit of Bernard Lyot: The Direct Detection of Planets and Circumstellar Disks in the 21st Century," Proc. of Conf. held 4-8 June 2007 at U.C. Berkeley, ed. P. Kalas

Najita, J.R., Carr, J.S., Strom, S.E., Watson, D.M., Pascucci, I., Hollenbach, D., Gorti, U., & L. Keller, 2010, ApJ, 712, 274

Najita, J.R., Doppmann, G.W., Bitner, M.A., Richter, M.J., Lacy, J.H., Jaffe, D.T., Carr, J.S., Meijerink, R., Blake, G.A., Herczeg, G.J.., & Glassgold, A.E. 2009, ApJ, 697, 957

Neufeld, D., et al. 2006, ApJ, 649, 816

Nidever, D. L., Marcy, G. W., Butler, R. P., Fischer, D. A., & Vogt, S. S. 2002, ApJS, 141, 503

Nomura, H., Aikawa, Y., Tsujimoto, M., Nakagawa, Y., & Millar, T. J. 2007, ApJ, 661, 334

Pascucci, I., Hollenbach, D., Najita, J., Muzerolle, J., Gorti, U., Herczeg, G.J., Hillenbrand, L.A., Kim, J.S., Carpenter, J.M., Meyer, M.R., Mamajek, E.E., & Bouwman, J. 2007, ApJ, 663, 383

Rieke, G. H., & Lebofsky, M. J. 1985, ApJ, 288, 618

Schwartz, R. D., & Greene, T. P. 2003, AJ, 126, 339

Straižys, V., Černis, K., & Bartašiūtė, S. 1996, Baltic Astronomy, 5, 125

Tine, S., Lepp, S., Gredel, R., & Dalgarno, A. 1997, ApJ, 481, 282

van Boekel, R., Güdel, M., Henning, Th., Lahuis, F., & Pantin, E. 2009, A&A, 497, 137

Weintraub, D. A., Kastner, J. H., & Bary, J. S. 2000, ApJ, 541, 767

White, R. J., & Hillenbrand, L. A. 2004, ApJ, 616, 998

Wilgenbus, D., Cabrit, S., Pineau des Forêts, G., & Flower, D. R. 2000, A&A, 356, 1010

Woitke, P. et al. 2009, in *Cool Stars, Stellar Systems, and the Sun: Proc. of the 15th Cambridge Workshop*, AIP Conf. Proc., 1094, 225

Zinnecker, H., McCaughrean, M. J., & Rayner, J. T. 1998, Nature, 394, 862

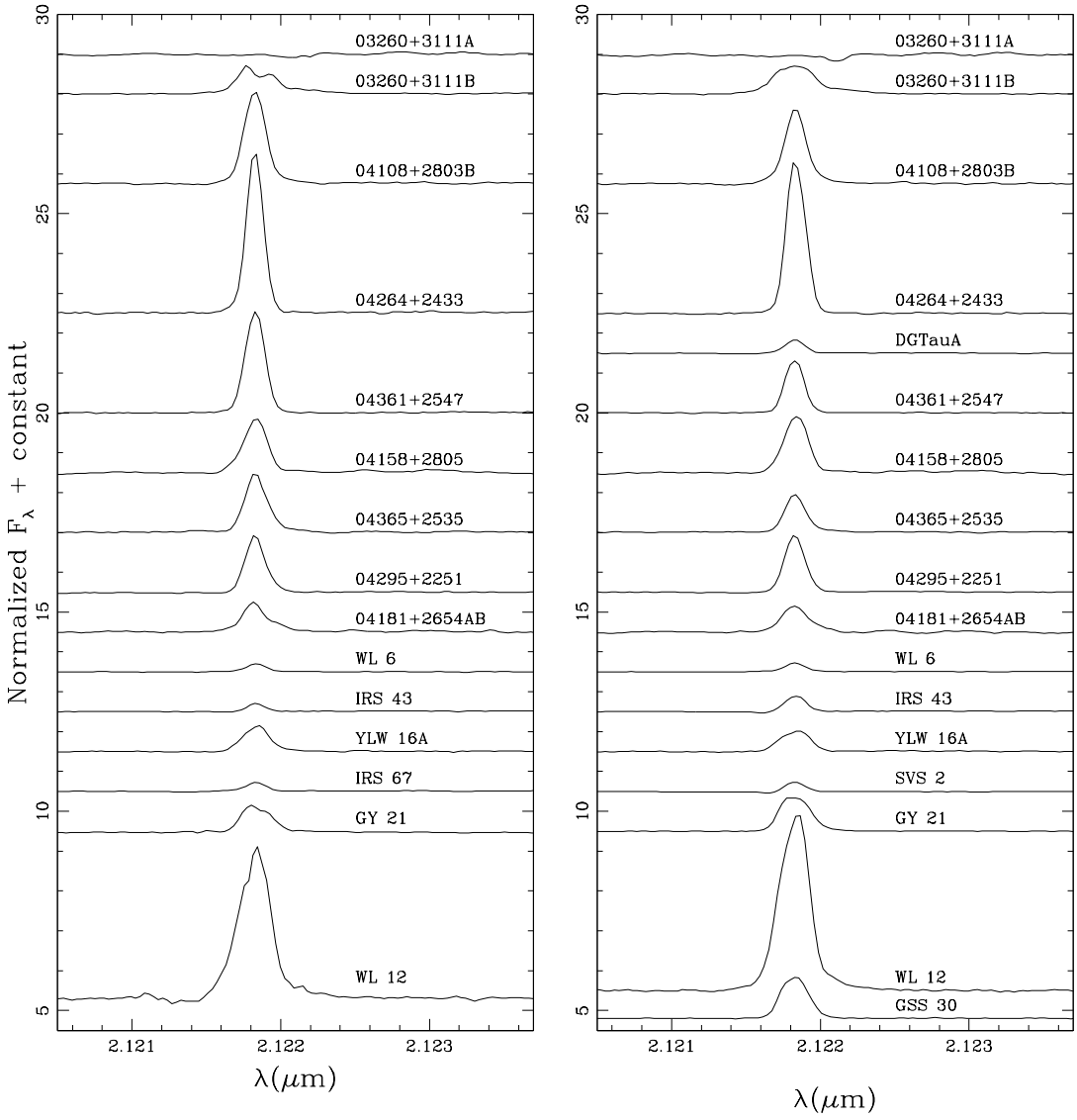

Fig. 1.— H_2 $v = 1 - 0$ $S(1)$ line spectra. Spectra acquired on 2007 Jun 24 and 2008 Jan 24 (first epoch) appear in the left panel, and spectra acquired on 2007 Jun 25 and 2008 Jan 25 (second epoch) appear in the right panel. These spectra were extracted only in the region containing the mostly point source continuum emission; any extended H_2 emission is not included.

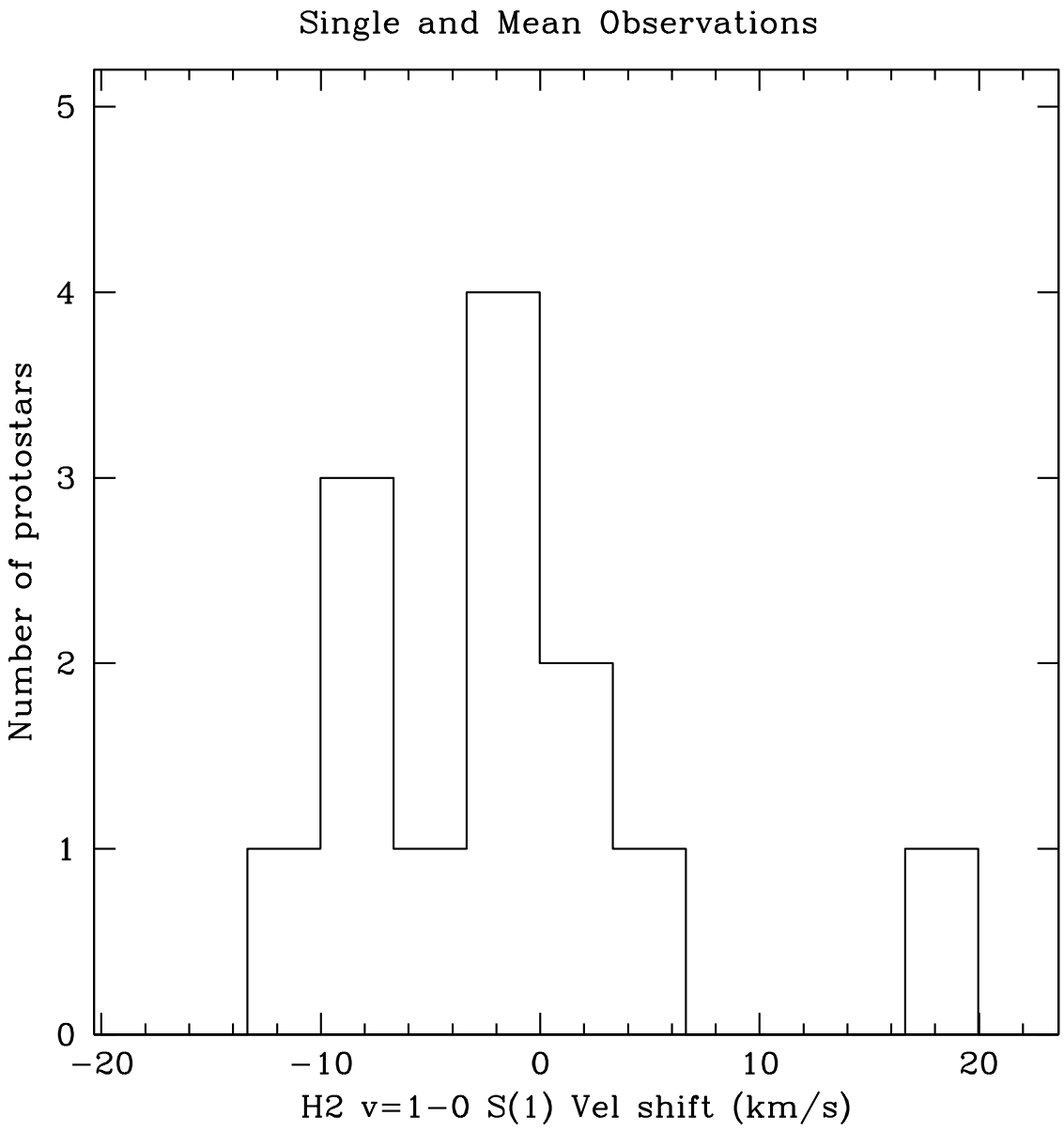

Fig. 2.— Histogram of mean H_2 $v = 1 - 0$ $S(1)$ line velocities minus photospheric velocities for all observations.

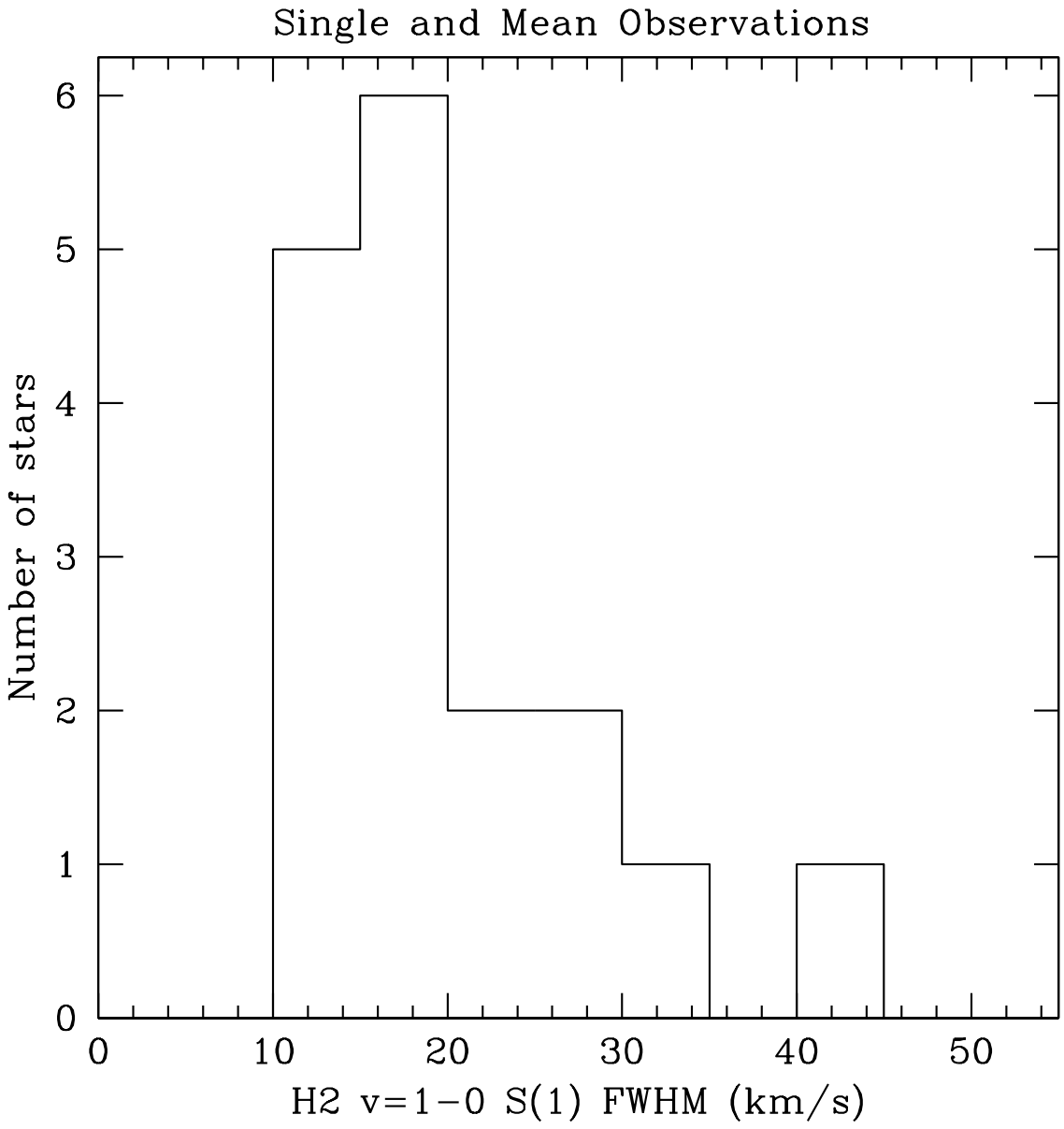

Fig. 3.— Histogram of H_2 $v = 1 - 0$ $S(1)$ line FWHM velocities. The instrumental line width of 17 km s^{-1} has been subtracted in quadrature from each value before binning.

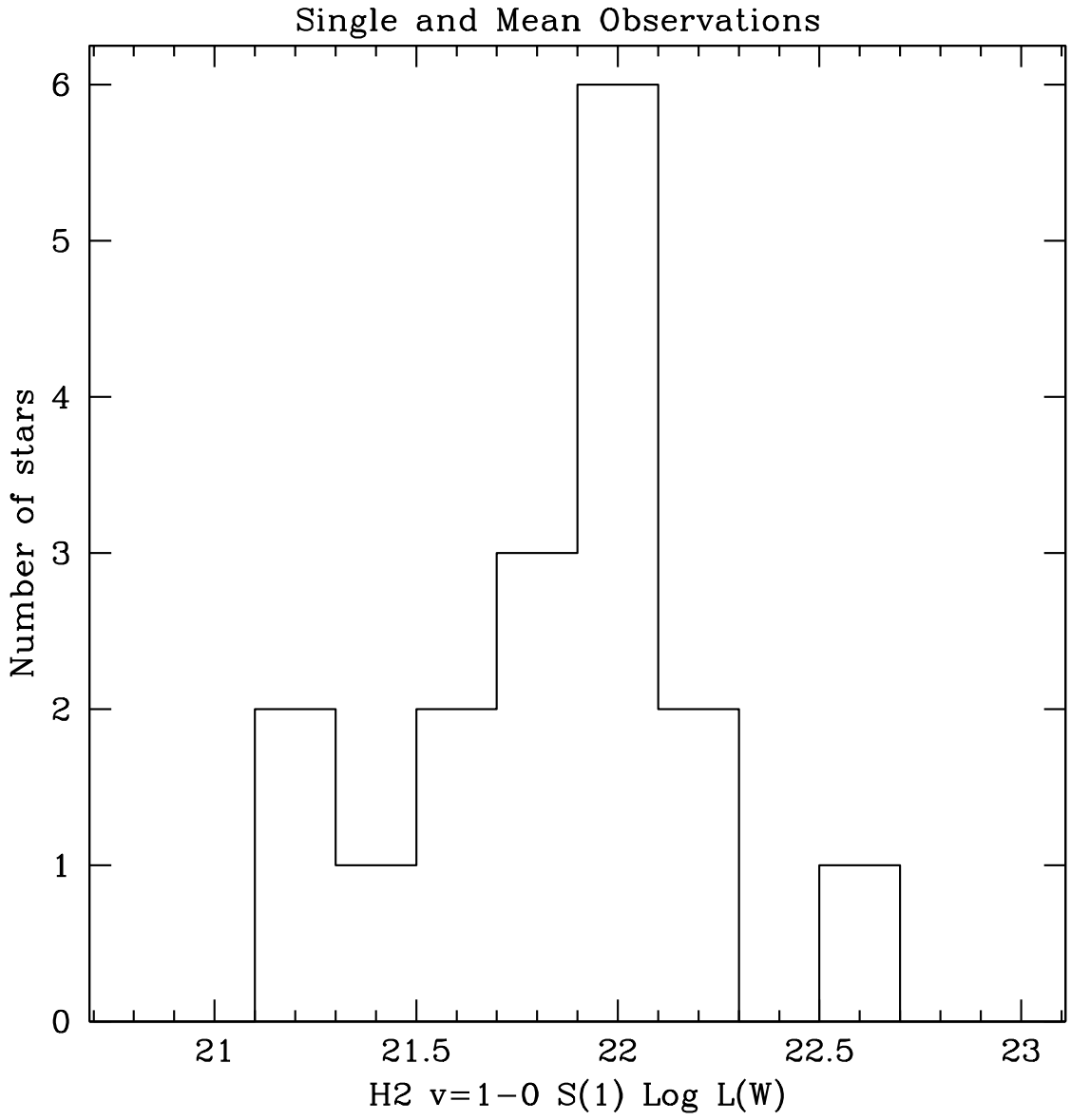

Fig. 4.— Histogram of H_2 $v = 1 - 0$ $S(1)$ line luminosities.

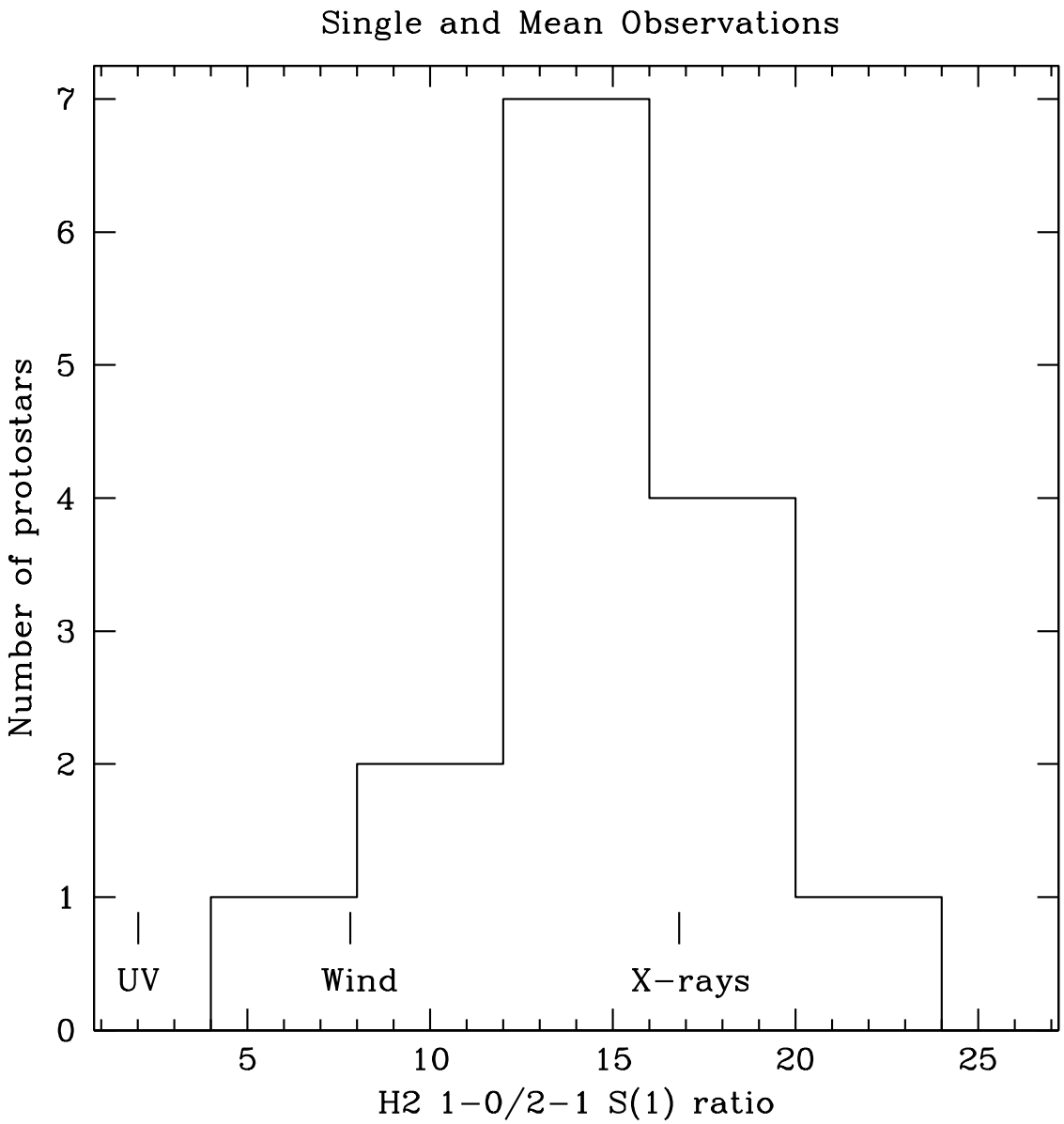

Fig. 5.— Histogram of H_2 $v = 1-0/2-1$ $S(1)$ line ratios. Values of 1.9, 7.7, and 17 are indicated, nominally correspond to UV, shock, and X-ray secondary electron impact excitation respectively in the presence of no dust (Gredel & Dalgarno 1995). These values are the inverse of those presented in column 8 of Table 2.

Table 1. Journal of Observations

Object	Region	α(J2000) (hh mm ss.s)	δ(J2000) (° ′ ″)	UT Date	Int. Time (minutes)	Slit PA (°E of N)
03260+3111B	Per	03 29 07.7	31 21 58	2008 Jan 24	20.0	103
				2009 Jan 25	20.0	149
03260+3111A	Per	03 29 10.7	31 21 59	2008 Jan 24	20.0	118
				2008 Jan 25	12.0	180
04108+2803B	Tau-Aur	04 13 54.9	28 11 31	2008 Jan 24	20.0	-123
				2008 Jan 25	25.0	121
04158+2805	Tau-Aur	04 18 58.2	28 12 24	2008 Jan 24	20.0	73
				2008 Jan 25	20.0	63
04181+2654AB	Tau-Aur	04 21 11.5	27 01 09	2008 Jan 24	10.0	48
				2008 Jan 25	30.0	172
DG Tau	Tau-Aur	04 27 04.8	26 06 17	2008 Jan 25	10.0	57
04264+2433	Tau-Aur	04 29 30.0	24 39 56	2009 Jan 24	12.0	57
				2008 Jan 25	12.0	-106
04295+2251	Tau-Aur	04 32 32.1	22 57 27	2009 Jan 24	40.0	-106
				2008 Jan 25	30.0	75
04361+2547	Tau-Aur	04 39 13.5	25 53 20	2008 Jan 24	12.0	68
				2008 Jan 25	12.0	-110
04365+2535	Tau-Aur	04 39 35.2	25 41 45	2008 Jan 24	44.0	97
				2008 Jan 25	33.3	99
GSS 30	Oph	16 26 21.4	-24 23 06	2007 Jun 25	14.0	-124
GY 21	Oph	16 26 23.6	-24 24 38	2007 Jun 24	20.0	-56
				2007 Jun 25	20.0	-100
WL 12	Oph	16 26 44.1	-24 34 48	2007 Jun 24	8.0	-47
				2007 Jun 25	10.0	-114
WL 6	Oph	16 27 21.6	-24 29 51	2007 Jun 24	20.0	-72
				2007 Jun 25	30.0	-89
IRS 43	Oph	16 27 27.0	-24 40 50	2007 Jun 24	45.0	-78
				2007 Jun 25	60.0	-66
YLW 16A	Oph	16 27 27.8	-24 39 32	2007 Jun 24	12.0	-85
				2007 Jun 25	12.0	-133
IRS 67	Oph	16 32 01.1	-24 56 45	2007 Jun 24	60.0	-59
SVS 2	Ser	18 29 56.8	01 14 46	2007 Jun 25	28.0	-85

Table 2. Protostar H_2 Line Analysis

Source	UT Date	1–0 S(0) EW (Å)[a]	1–0 S(1) EW (Å)[a]	2–1 S(1) EW (Å)[a]	A_v[b] (mag)	1–0 S(1) Log L(W)	2–1/1–0 S(1)	FWHM[c] (km s^{-1})	V(H_2 - *)[d] (km s^{-1})	H_2 1–0 S(1) extent (″)
03260+3111B	2008 Jan 24[e]	0.50	2.12	0.49	3.5	22.0	0.25	43	...	$\gtrsim 10$
	2008 Jan 25	0.51	2.69	0.39	3.5	22.1	0.14	44	...	$\lesssim 1$
03260+3111A[f]	2008 Jan 24	< 0.1	< 0.1	< 0.1	...	...	...	...	...	~ 7
	2008 Jan 25	< 0.1	< 0.1	< 0.1	...	...	...	...	...	$\gtrsim 10$
04108+2803B	2008 Jan 24	0.92	4.29	0.39	19	22.0	0.08	18	-1	~ 1
	2008 Jan 25	0.69	3.43	0.29	19	21.9	0.07	18	-1	~ 1
04158+2805	2008 Jan 24	0.49	2.57	0.26:	3.1	21.1	0.08:	20	-4	< 1
	2008 Jan 25	0.35	2.70	0.22:	3.1	21.2	0.06:	20	-4	~ 2
04181+2654AB	2008 Jan 24	0.23	1.46	0.04::	23	22.0	...	24	-1	~ 1
	2008 Jan 25	0.39	1.37	0.00::	23	21.9	...	25	8	< 1
DG Tau	2008 Jan 25	0.14	0.54	0.06::	0	22.0	0.08::	14	-9	< 1
04264+2433	2008 Jan 24	1.56	5.78	0.53	6.1	21.7	0.06	10	4	~ 2
	2008 Jan 25	1.44	6.09	0.52	6.1	21.7	0.06	13	-4	6
04295+2251	2008 Jan 24	0.59	2.42	0.14:	17	22.0	0.04:	16	...	~ 2
	2008 Jan 25	0.59	2.43	0.16:	17	22.0	0.05:	16	...	~ 2
04361+2547	2008 Jan 24	1.06	4.11	0.45	22	22.2	0.08	14	...	0

Table 2—Continued

Source	UT Date	1–0 S(0) EW (Å)[a]	1–0 S(1) EW (Å)[a]	2–1 S(1) EW (Å)[a]	A_v[b] (mag)	1–0 S(1) Log L(W)	2–1/1–0 S(1)	FWHM[c] (km s^{-1})	V(H_2 - *)[d] (km s^{-1})	H_2 1–0 S(1) extent (″)
	2008 Jan 25	0.66	2.10	0.21:	22	21.9	0.07:	13	...	0
04365+2535	2008 Jan 24	0.57	2.58	0.18:	19	21.9	0.06:	19	...	0
	2008 Jan 25	0.35	1.59	0.09:	19	21.6	0.05:	16	...	0
GSS 30	2007 Jun 25	0.53	2.35	0.20	20	22.6	0.07	25	-11	2
GY 21[g]	2007 Jun 24	0.37	1.80	0.20	16	21.8	0.07	28	-11	∼ 1
	2007 Jun 25	0.52	2.21	0.20	16	21.9	0.07	29	-10:	∼ 1
WL 12	2007 Jun 24	1.43	12.4	0.79	18	22.1	0.06	32	-2	∼ 2
	2007 Jun 25	2.06	11.0	0.73	18	22.1	0.06	29	-12	∼ 1
WL 6	2007 Jun 24	0.06:	0.34	0.06:	37	21.6	0.15:	15	0	0
	2007 Jun 25	0.09	0.37	0.03:	37	21.6	0.07:	16	-3	0
IRS 43[h]	2007 Jun 24	0.09	0.28	0.02::	33	21.8	0.05::	9	0	∼ 3
	2007 Jun 25	0.17	0.64	0.04:	33	22.1	0.05::	22	-4	∼ 3
YLW 16A	2007 Jun 24	0.32	1.41	0.20	17	21.6	0.12	25	0	∼ 2
	2007 Jun 25	0.31	1.25	0.13	17	21.6	0.09	28	-4	∼ 3
IRS 67	2007 Jun 24	0.13	0.37	0.03::	22	21.1	0.07::	15	0	∼ 1

Table 2—Continued

Source	UT Date	1–0 S(0) EW (Å)[a]	1–0 S(1) EW (Å)[a]	2–1 S(1) EW (Å)[a]	A_v[b] (mag)	1–0 S(1) Log L(W)	2–1/1–0 S(1)	FWHM[c] (km s^{-1})	V(H_2 - *)[d] (km s^{-1})	H_2 1–0 S(1) extent (″)
SVS 2[i]	2007 Jun 25	0.09	0.39	0.01:::	0	21.5	...	13	19	~ 3

[a]Positive equivalent widths indicate emission. Uncertainties are $\sim 0.02\AA$ for 2007 data and $\sim 0.05\AA$ for 2008 data.

[b]V magnitude extinction was computed using each objects 2MASS JHK colors, an extinction law, and estimated intrinsic CTTS locus colors as explained in the text in §3.4

[c]The mean FWHM velocity of the 1–0 S(1) H_2 line, where the intrinsic instrumental line width of 17 km s^{-1} has been removed in quadrature.

[d]The radial velocity of the stellar photosphere subtracted from the mean radial velocity of the 1–0 S(0), 1–0 S(1), and 2–1 S(1) H_2 emission lines (uncertain lines not used). No data indicate that the star lacked either H_2 or photospheric lines.

[e]Spectrum displays $\Delta v = 2 - 0$ CO emission.

[f]Extended H_2 emission is spatially displaced from the star. No H_2 emission is coincident with the stellar continuum (as also observed by Doppmann et al. 2005).

[g]The H_2 emission slightly spatially displaced from the stellar continuum has velocity FWHM $\Delta v \sim 60$ km s^{-1}, about twice that of the H_2 emission spatially coincident with the stellar continuum.

[h]Extended H_2 emission shows velocity structure with a maximum FWHM $\Delta v \sim 40$ km s^{-1}, about twice that of the H_2 emission spatially coincident with the stellar continuum.

[i]The extended H_2 emission is separated from the stellar continuum and its line emission by $\sim 2''$. The extended emission has FWHM $\Delta v \sim 24$ km s^{-1}, about twice that of the H_2 emission spatially coincident with the stellar continuum. H_2 line strength

ratio was not calculated due to the very low value and high uncertainty ($\sim 50\%$) of the 2–1 S(1) line measurement.